Laboratório de Aerodinâmica
Departamento de Engenharia Aeronáutica
USP-São Carlos

EESC • USP
São Carlos School of Engineering
University of São Paulo

ENGENHARIA AERONÁUTICA
USP • SÃO CARLOS

Drag Breakdown and Tip Vortex Structure Analysis of a Camber Morphing Winglet

Professor Fernando Martini Catalano
PhD student João Paulo Eguea
PhD student Pedro David Bravo Mosquera

7th UTIAS International Workshop on Aviation and Climate Change, May 19-21, 2021

Background

- New configurations studies
  - Blended wingbody

Ceron-Muñoz, H. D, Catalano F.M. The Aerodynamic Interference of power plant system on a Blended Wing Body. 27T H International
Congress of the Aeronautical Sciences, Nice,

France, 2010.

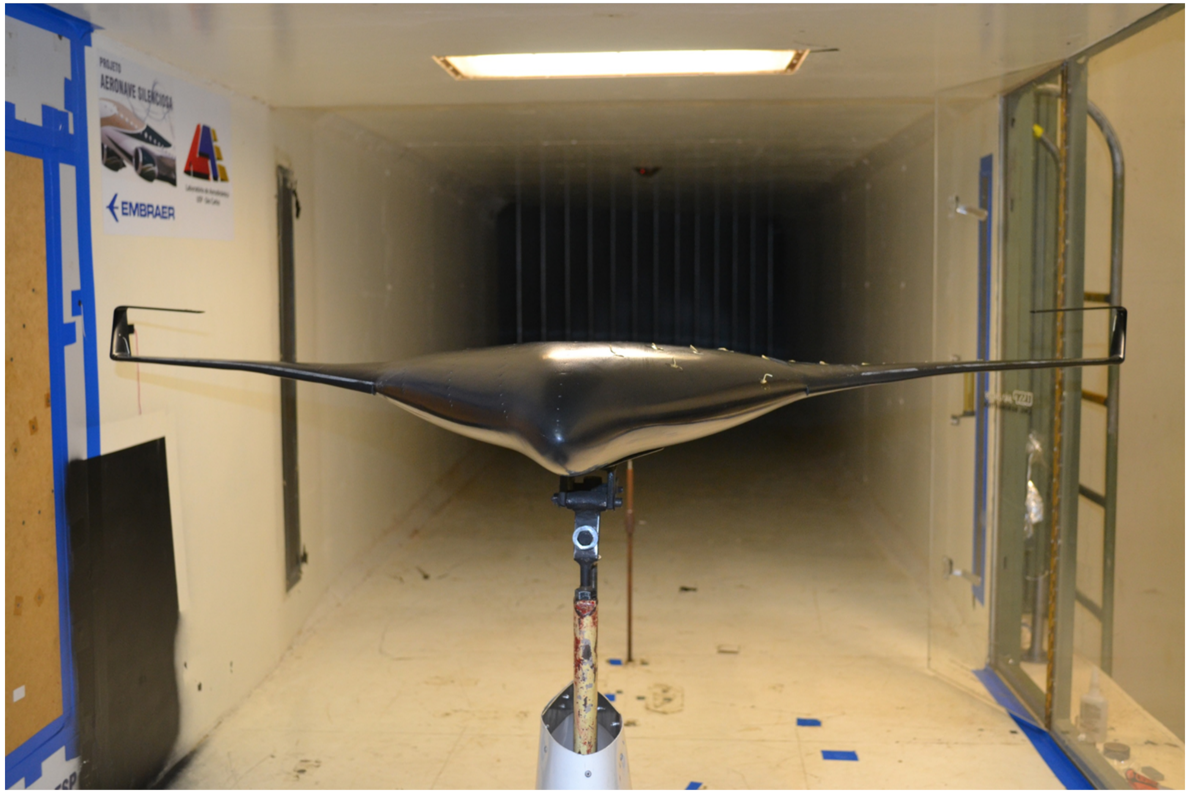

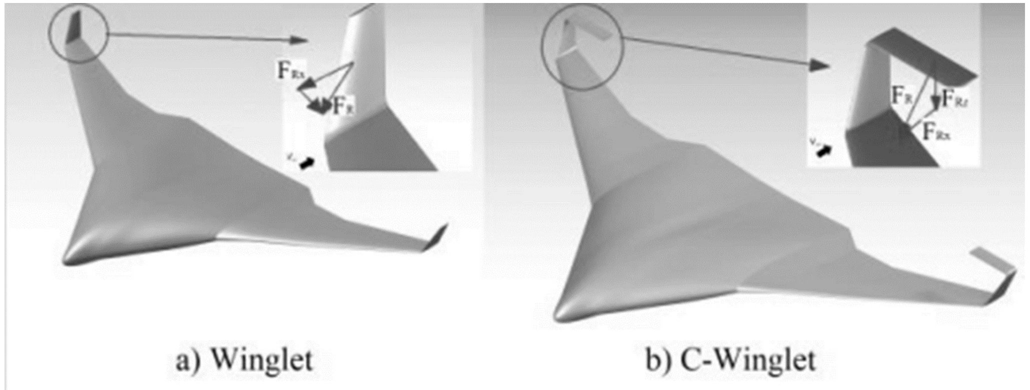

AERODYNAMIC INTERFERENCE OF WINGTIP AND WING DEVICES ON BWB MODEL
H. D. Ceron-Muñoz∗ , D. O. Diaz-Izquierdo, J. Solarte-Pineda, F. M. Catalano∗ ICAS 2014

Design, aerodynamic optimization and experimental assessment of a next generation commercial airliner

- Focused on the combination of two revolutionary technologies: Box-wing and BLI ingestion

- Single-aisle category

- Conceptual-level MDO studies

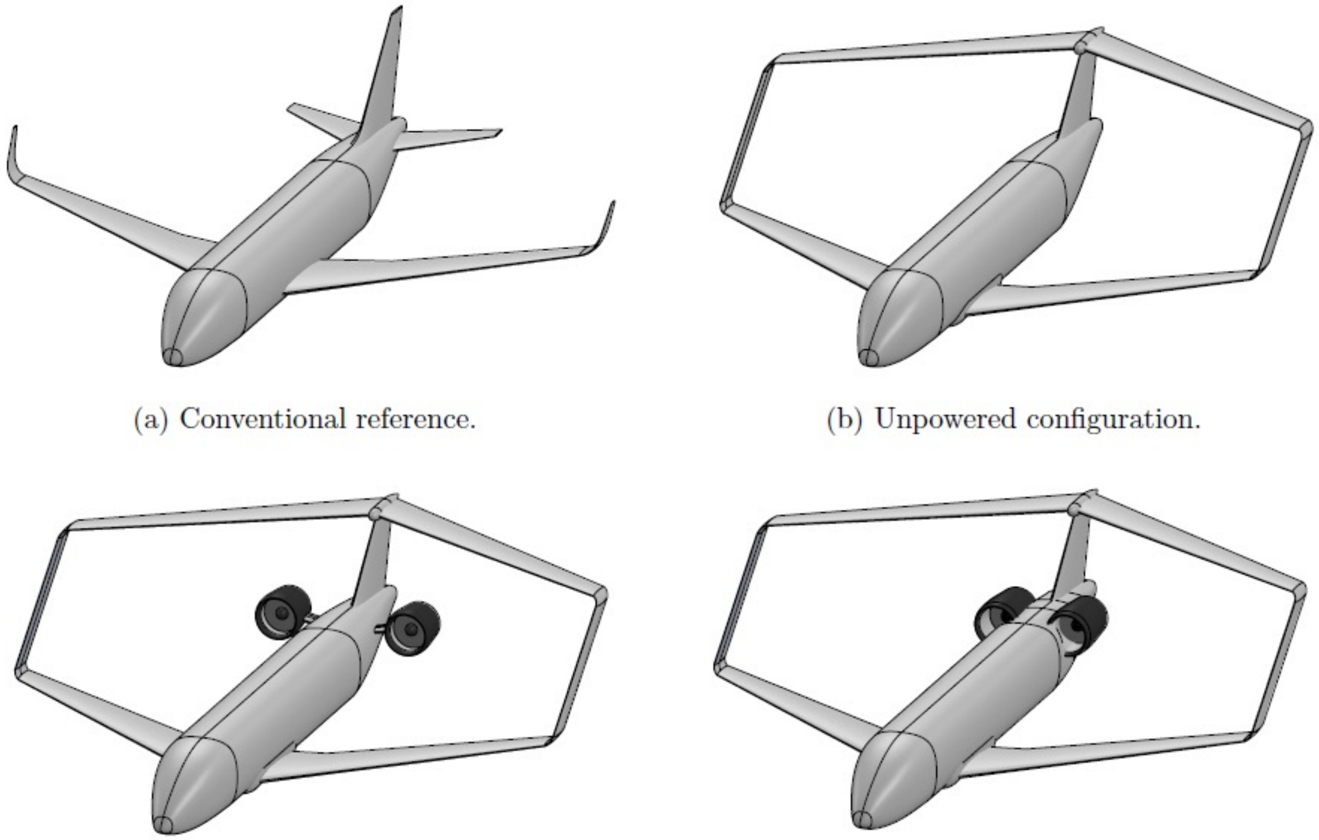

(a) Conventional reference.

(b) Unpowered configuration.

(c) Non-BLI configuration.

(d) BLI configuration.

CFD analysis

- Mach 0.78, optimum cruise altitude
- Propulsion modeled as an actuator disk

- Power saving 6.55%
- Fuel-burn benefits of about 15%

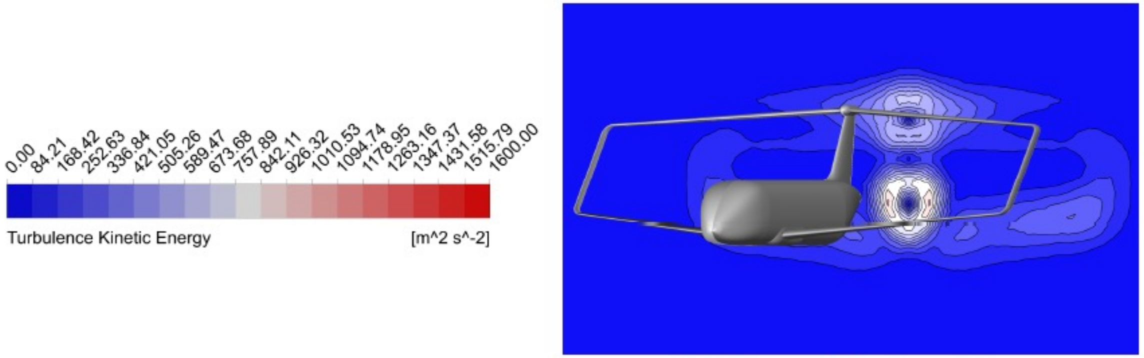

(a) Unpowered configuration.

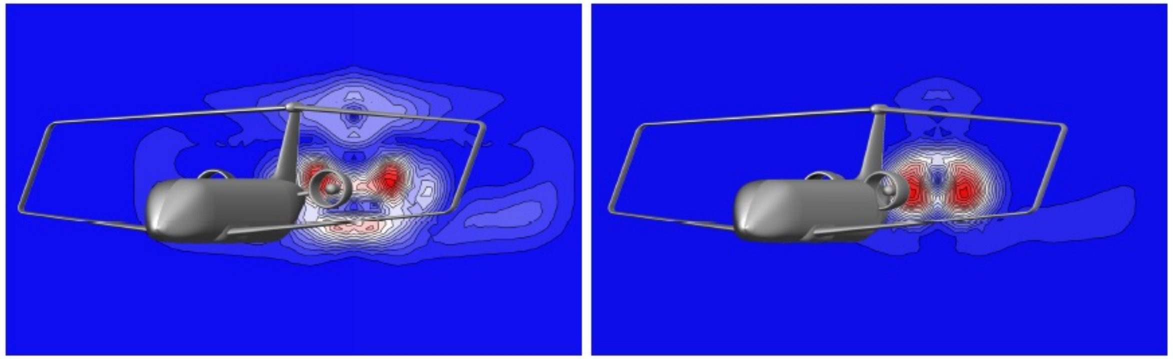

(b) Non-BLI configuration.

(c) BLI configuration.

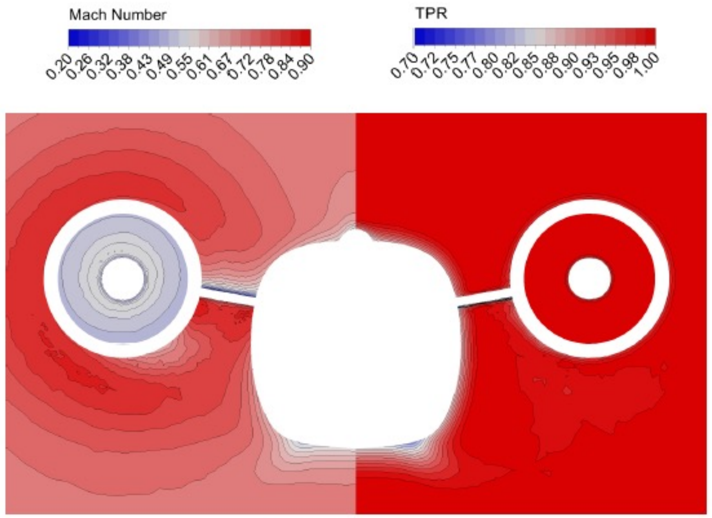

(a) Non-BLI version.

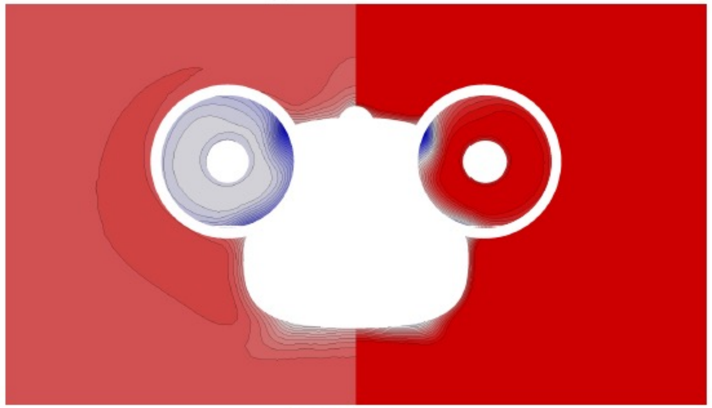

(b) BLI version.

Subsonic wind-tunnel experiments

- Conventional force balance and power balance measurements
- 7-hole probe measurements to visualize the flow
- Total pressure surveys using a distortion rake

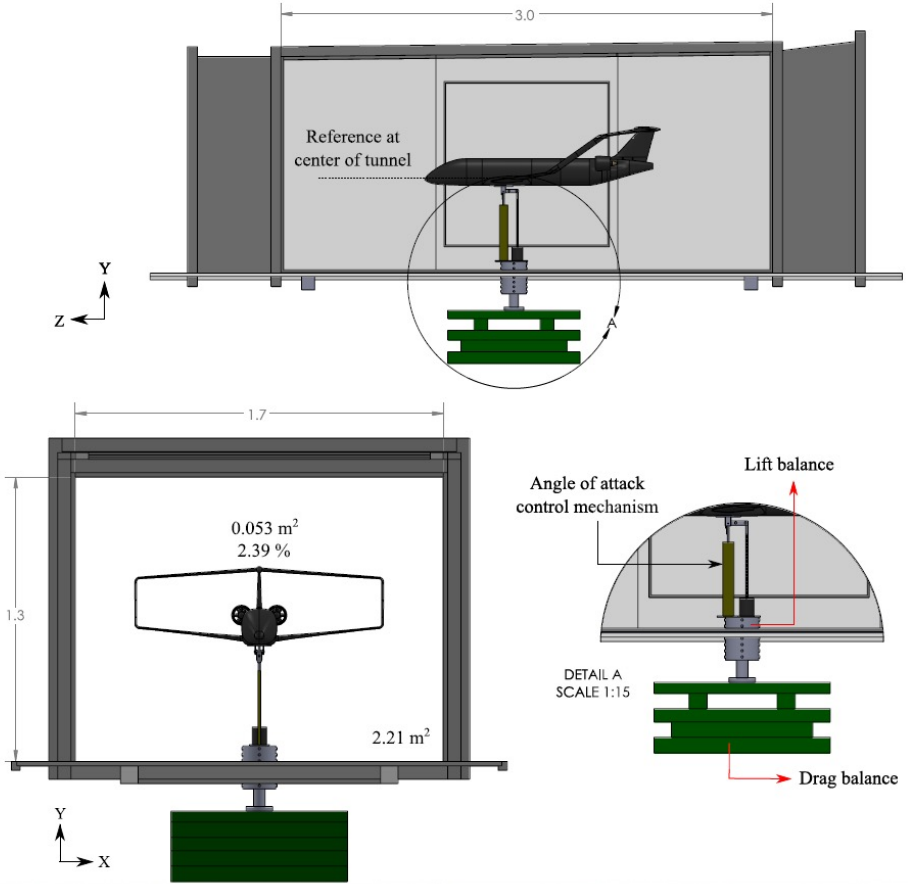

- Background
- Laminar wing testing Pusher propeller effect

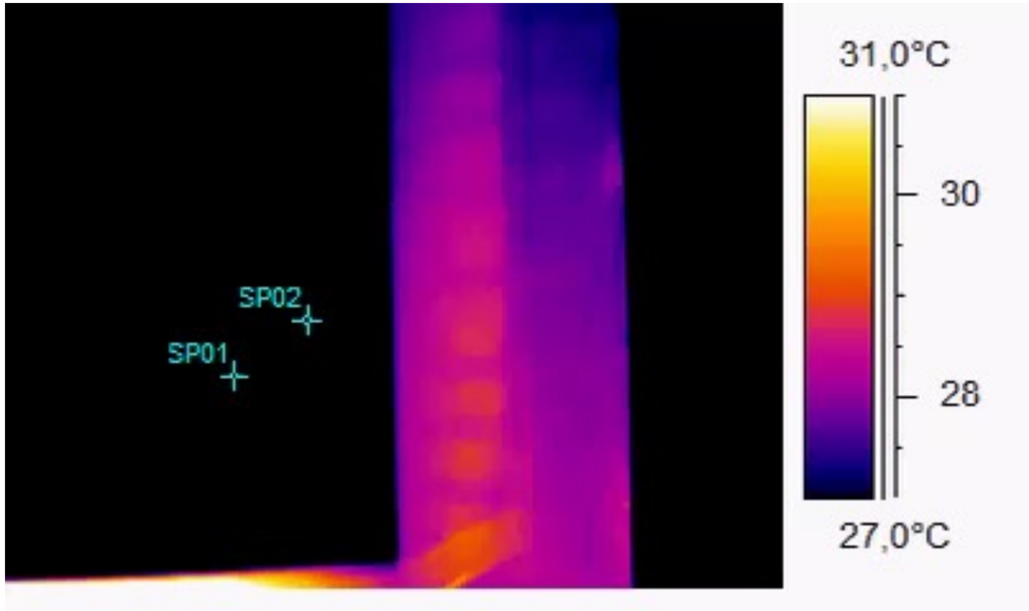

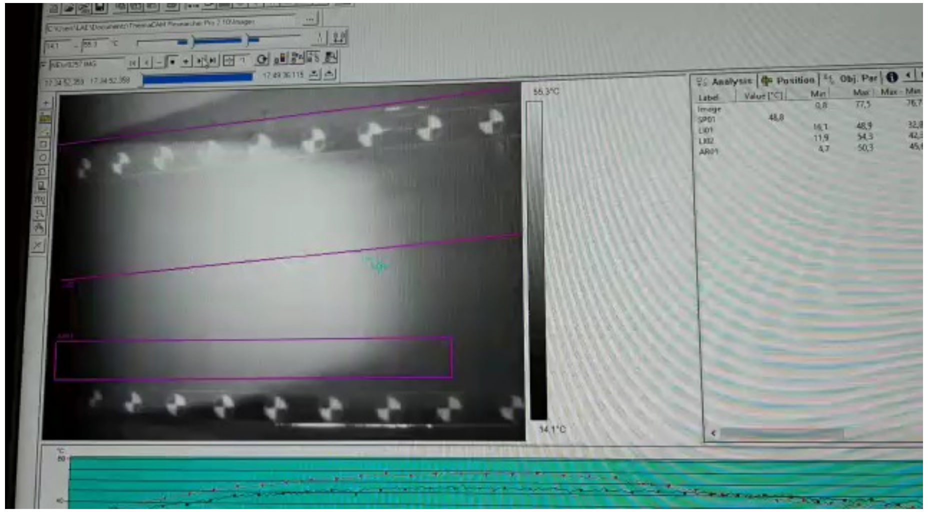

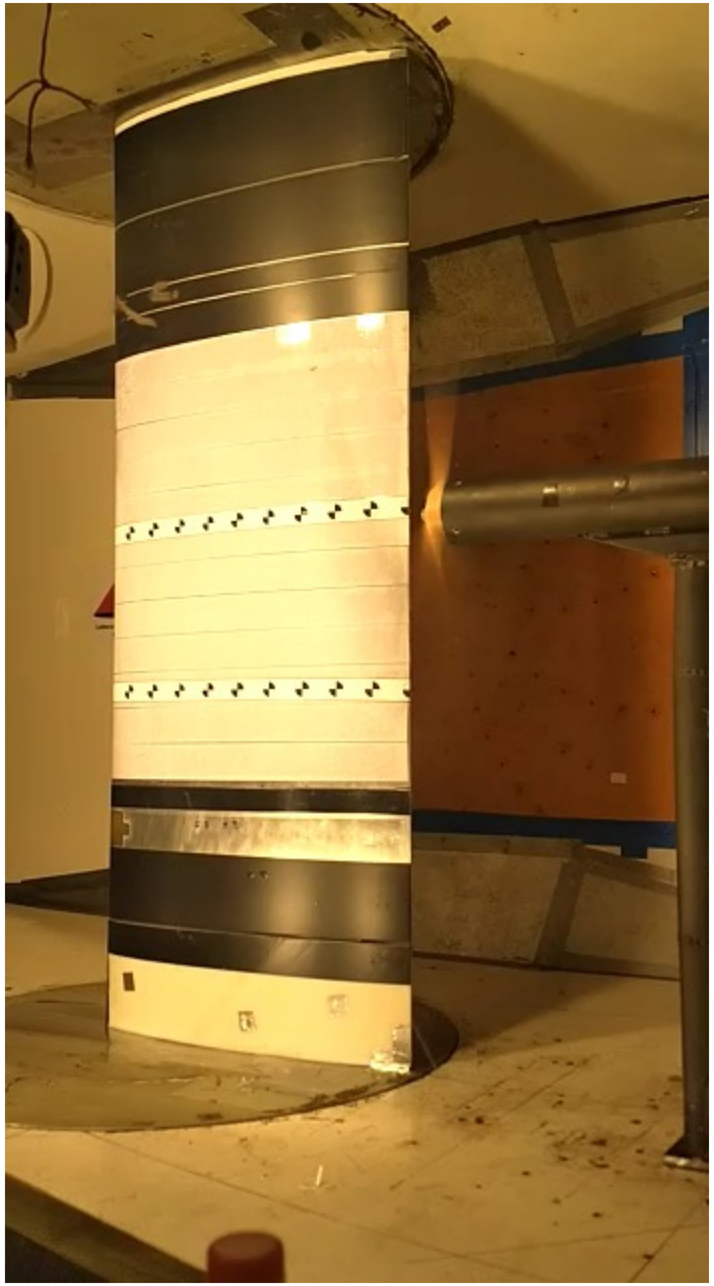

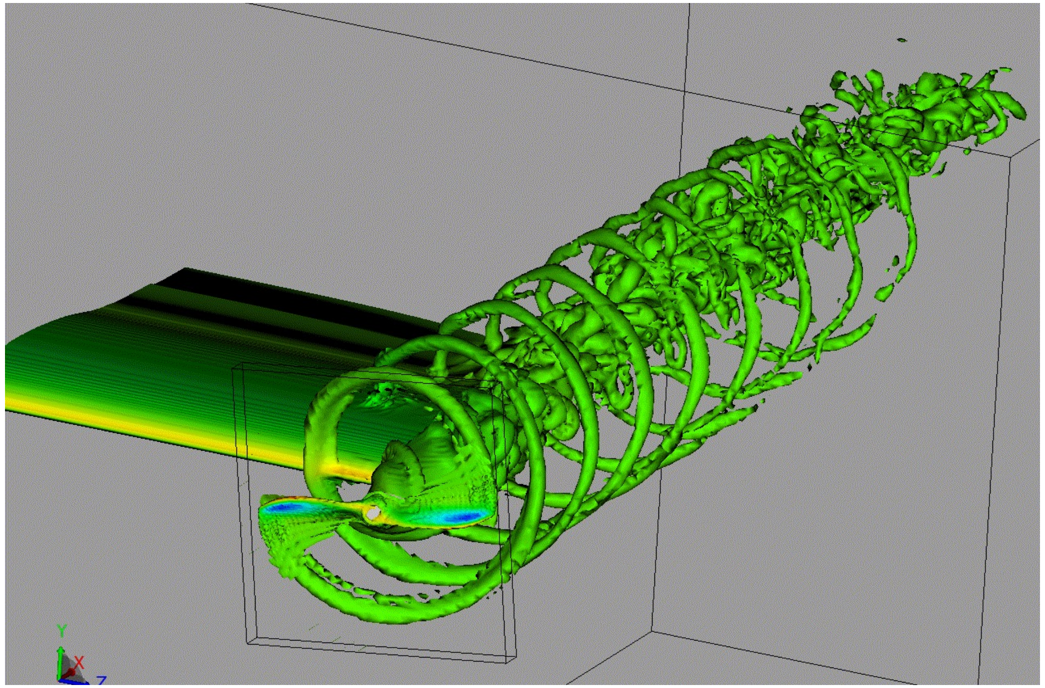
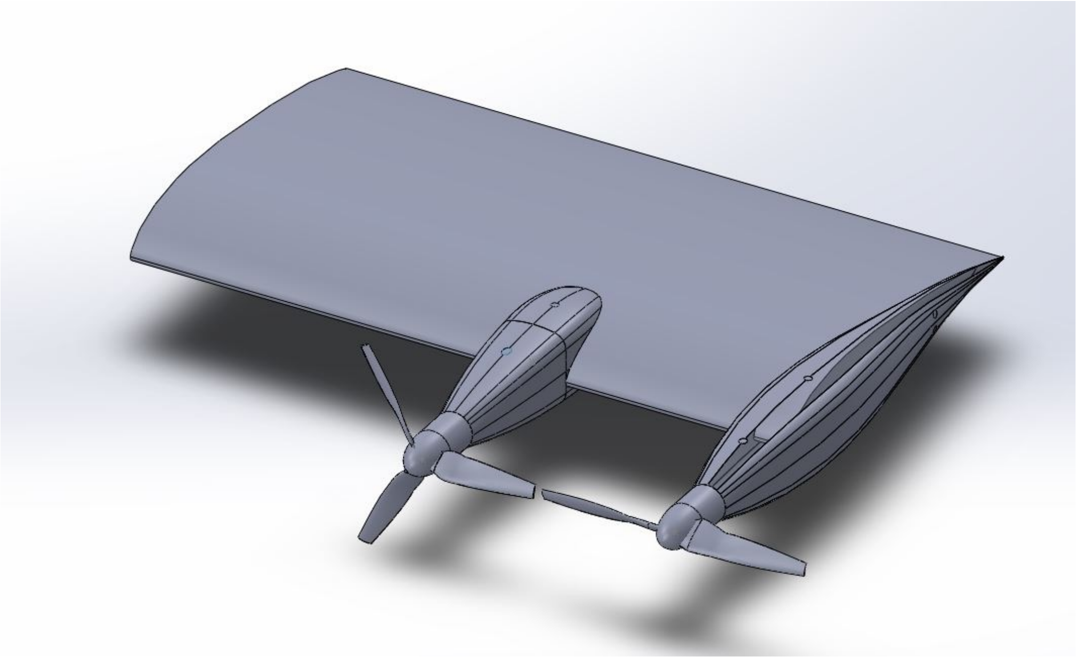
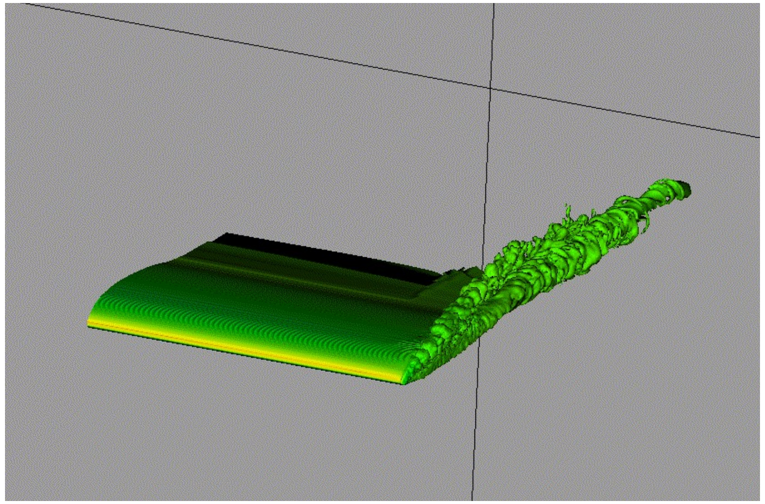
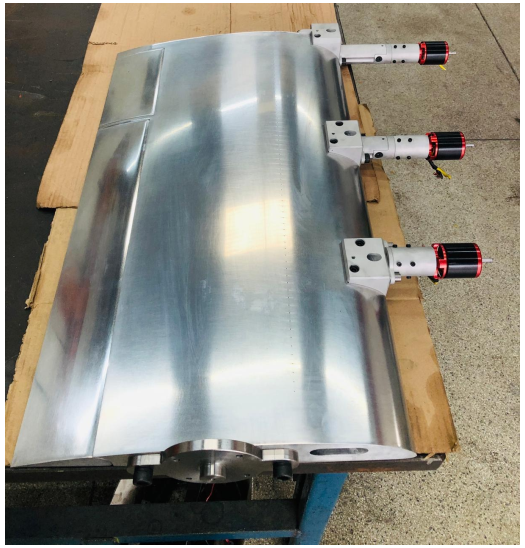

Distributed propulsion aerodynamics and aeroacoustics

DEVELOPMENT OF A BLOWING SYSTEM FOR A PYLON-PUSHER PROPELLER CONFIGURATION WITH THE STUDY OF THE ASSOCIATED AERODYNAMIC AND AEROACOUSTIC PHENOMENA

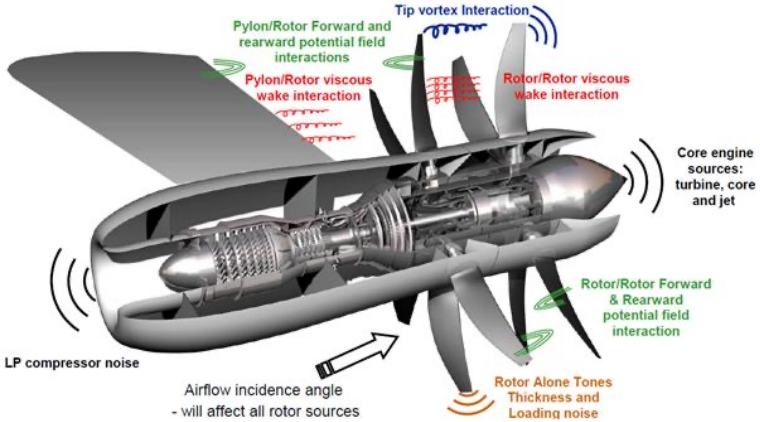

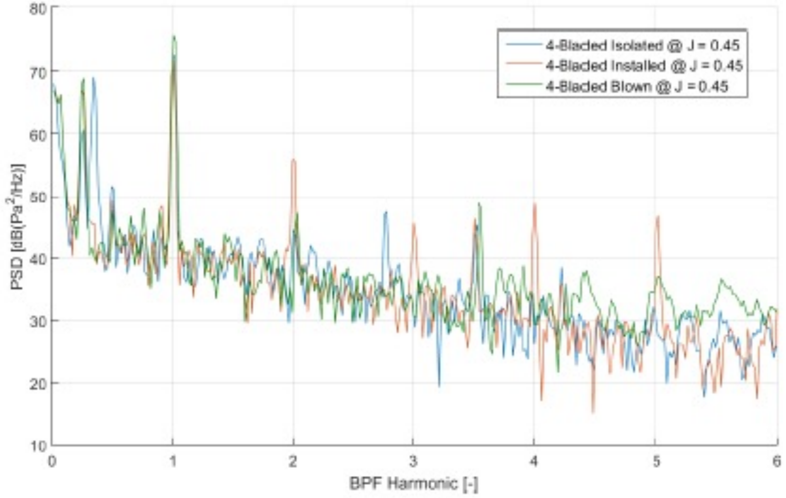

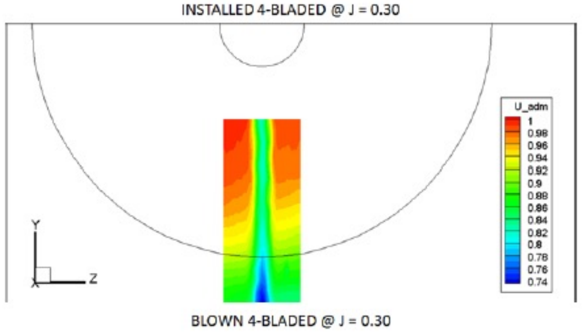

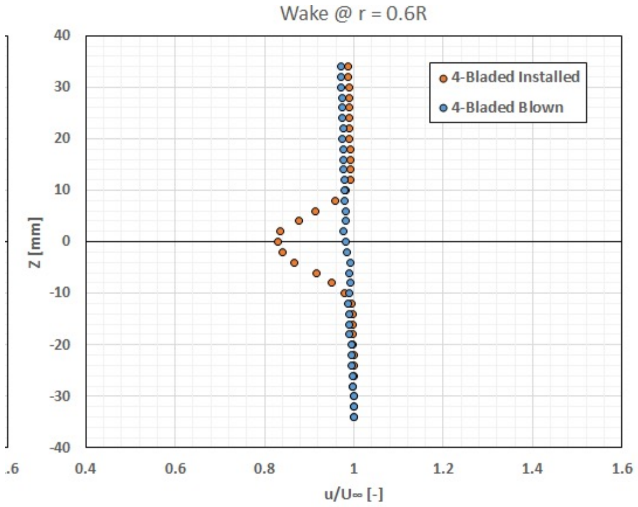

Noise Reductions on a Pusher Propeller Configuration through Pylon Tangential Blowing
LF Rego, LT Lima Pereira, F Catalano
2018 AIAA/CEAS Aeroacoustics Conference, 4194

Experimental Investigation of Wing-Tip Devices on the Reduction of Induced Drag

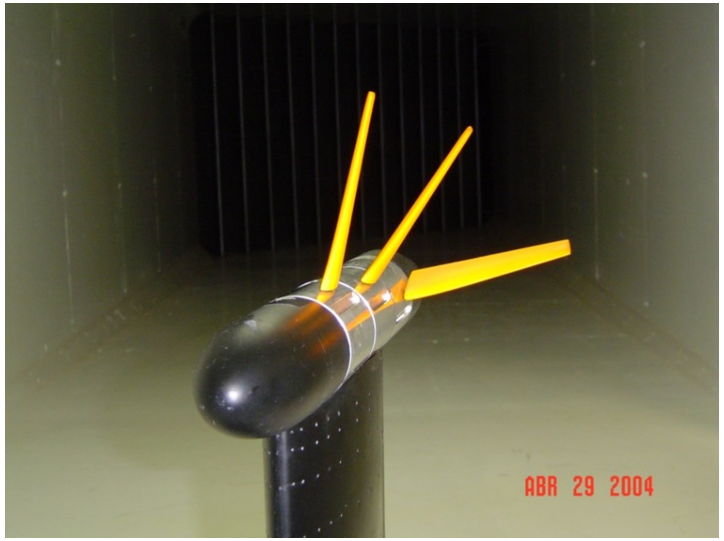

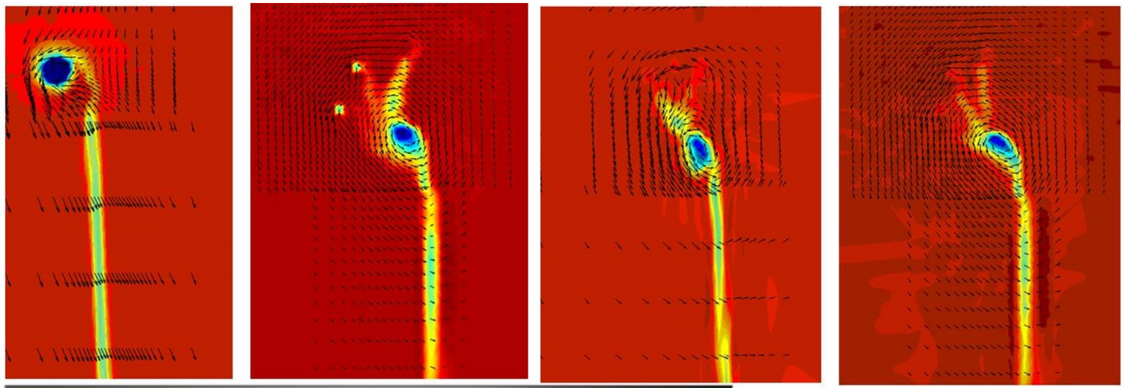

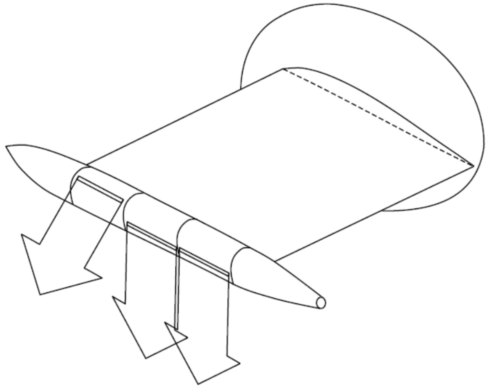

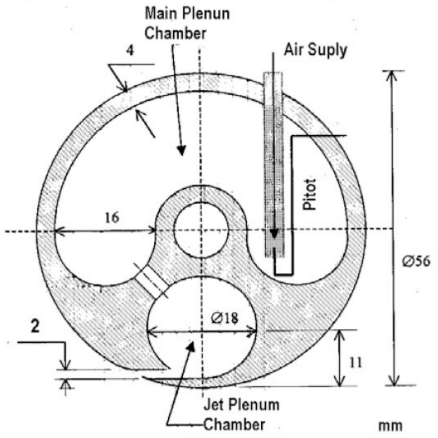

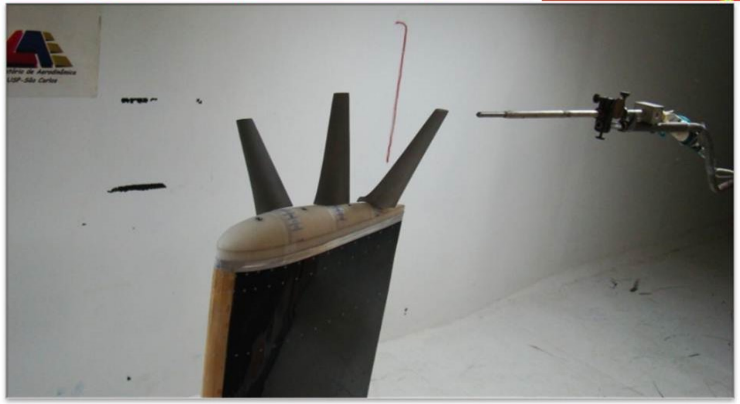

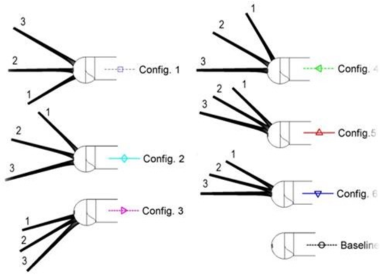

Experimental investigation of wing-tip devices on the reduction of induced drag
HD Céron-Muñoz, R Cosin, RFF Coimbra, LGN Correa, FM Catalano
Journal of Aircraft 50 (2), 441-449

Flap side-edge noise reduction

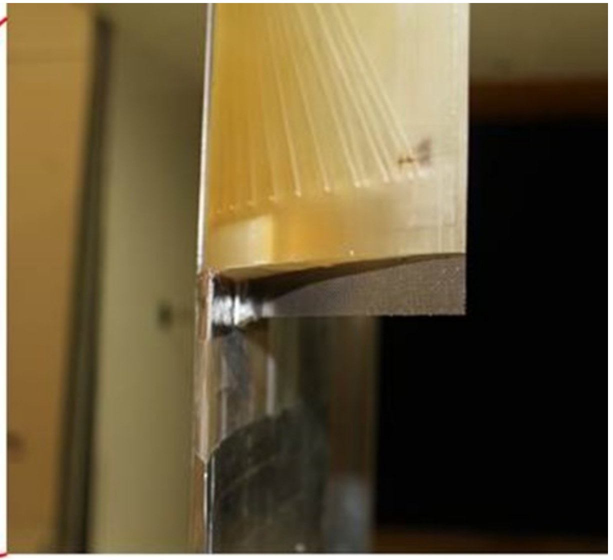

Mophing wing or variable camber wing

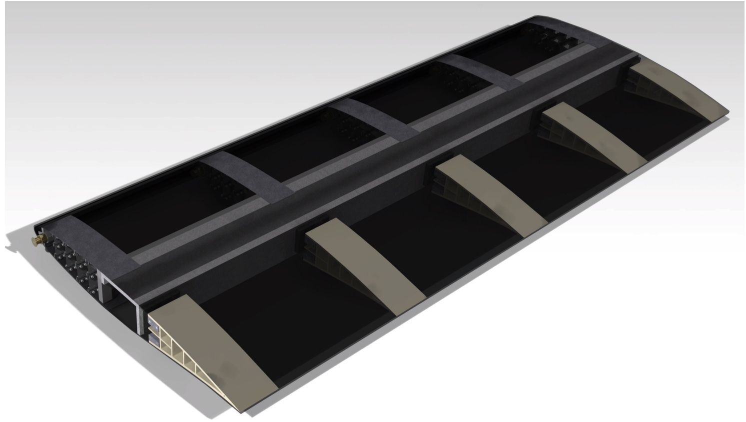

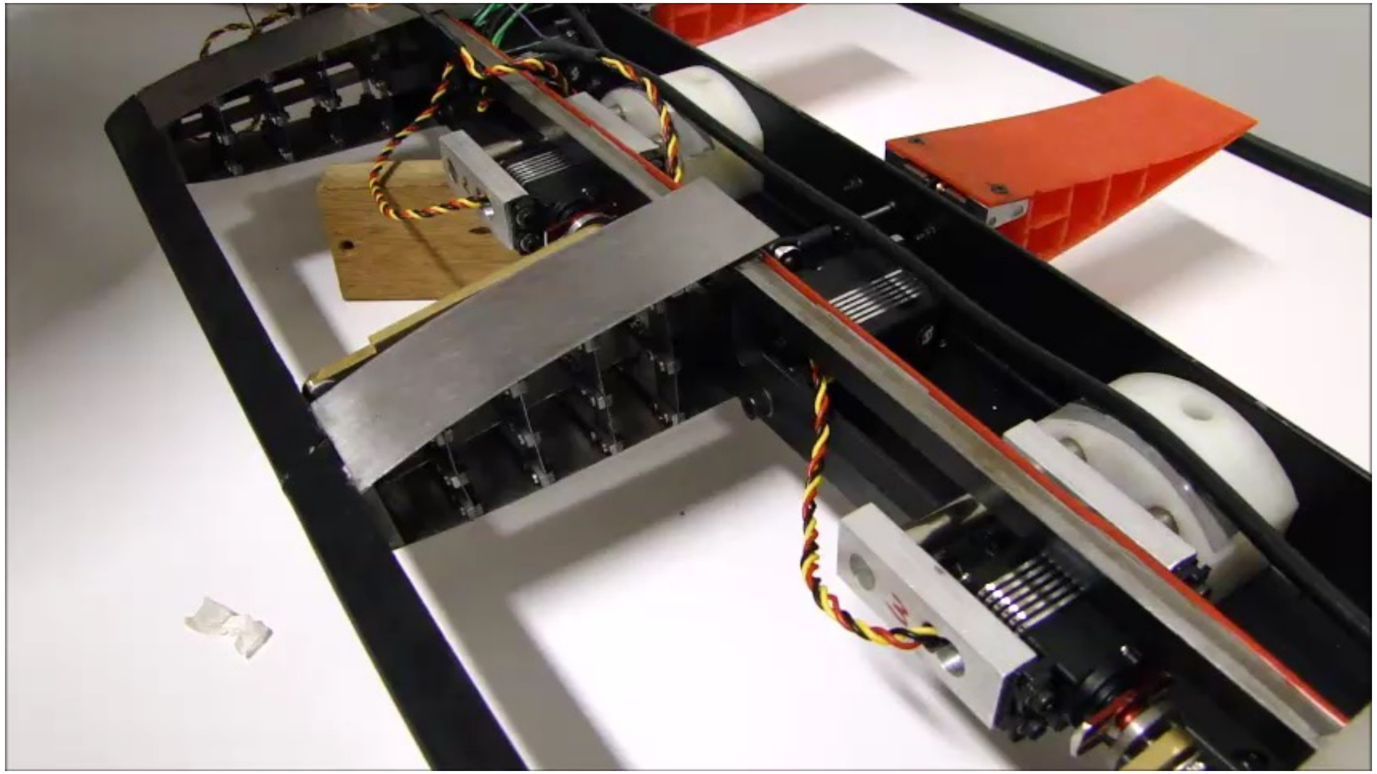

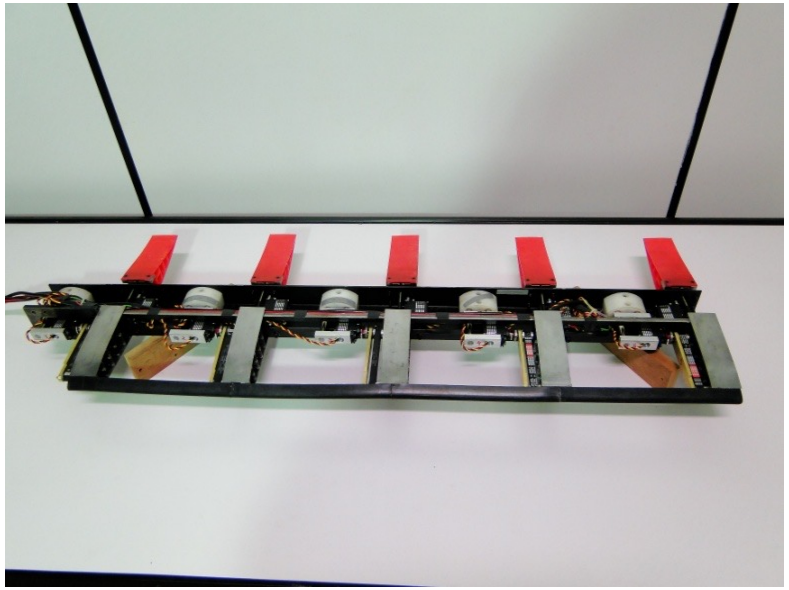

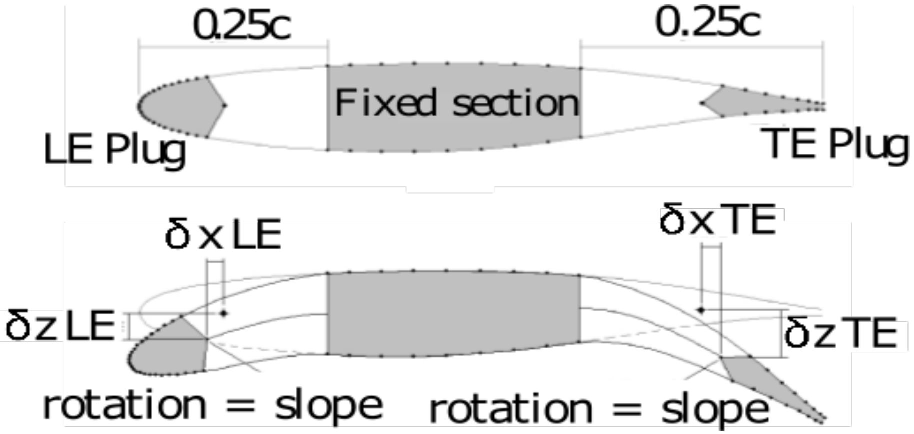

J. Braz. Soc. Mech. Sci. & Eng. vol.25 no.1 Rio de Janeiro Jan./Mar. 2003
http://dx.doi.org/10.1590/S1678-58782003000100001
Drag optimization for transport aircraft Mission Adaptive Wing
A. L. Martins; F. M. CatalanoI

Drag Breakdown and Tip Vortex Structure Analysis of a Camber Morphing Winglet

Motivation to apply morphing systems to a wing let:

- Less critical component
- Small changes on overall configuration
- Performance improvement – Induced drag reduction

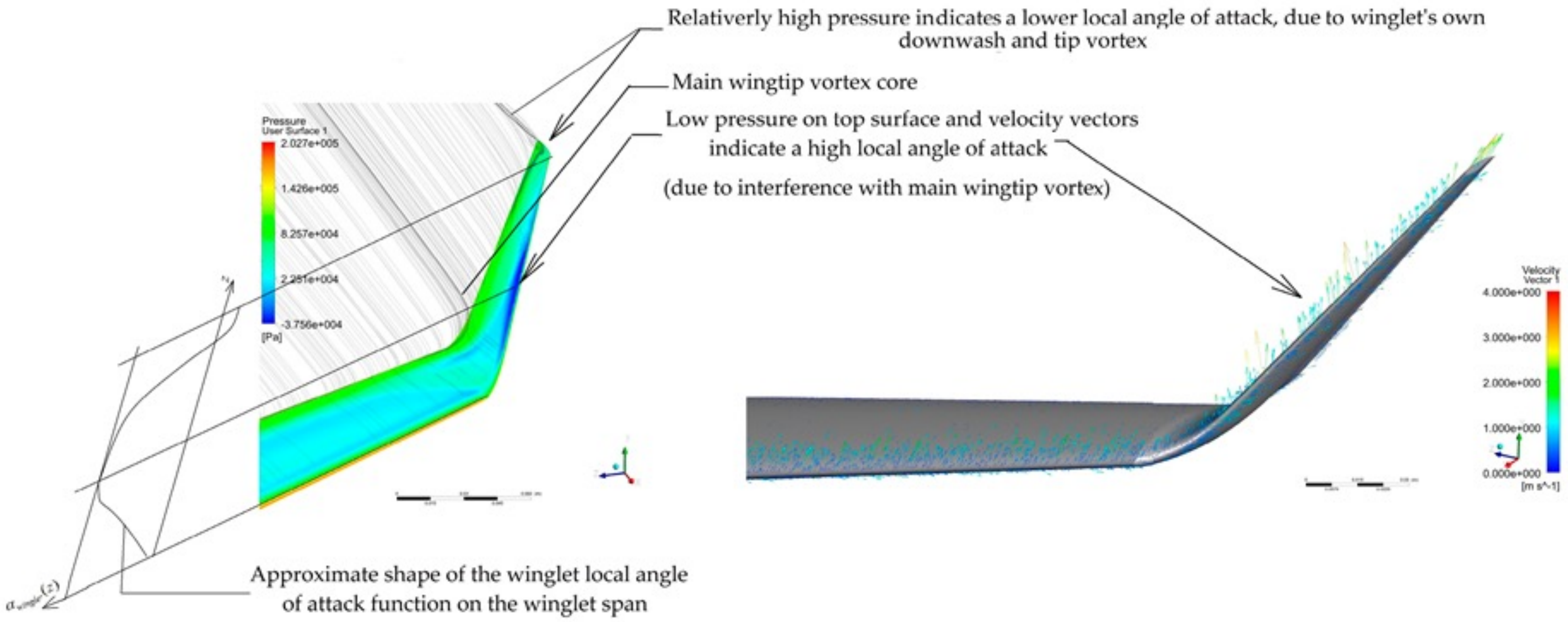

Relativerly high pressure indicates a lower local angle of attack, due to winglet's own downwash and tip vortex
Main wingtip vortex core
Low pressure on top surface and velocity vectors indicate a high local angle of attack
(due to interference with main wingtip vortex)
Pressure
User Surface 1
2.027e+005
1.426e+005
8.257e+004
2.281e+004
-3.756e+004
[Pa]
Velocity
Vector 1
4.000e+000
3.000e+000
2.000e+000
1.000e+000
0.000e+000
[m s^-1]
Approximate shape of the winglet local angle of attack function on the winglet span

Concept evaluation

- Optimized fixed geometry winglet (FGW) x camber morphing winglet (CMW)

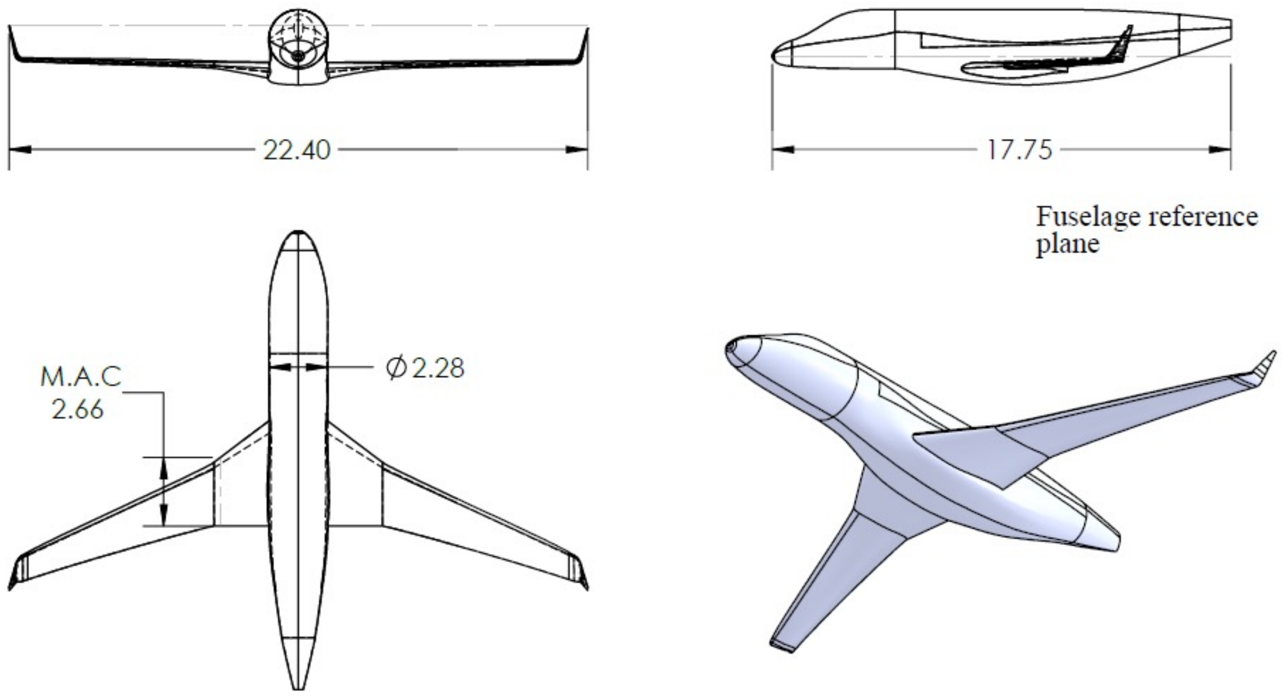

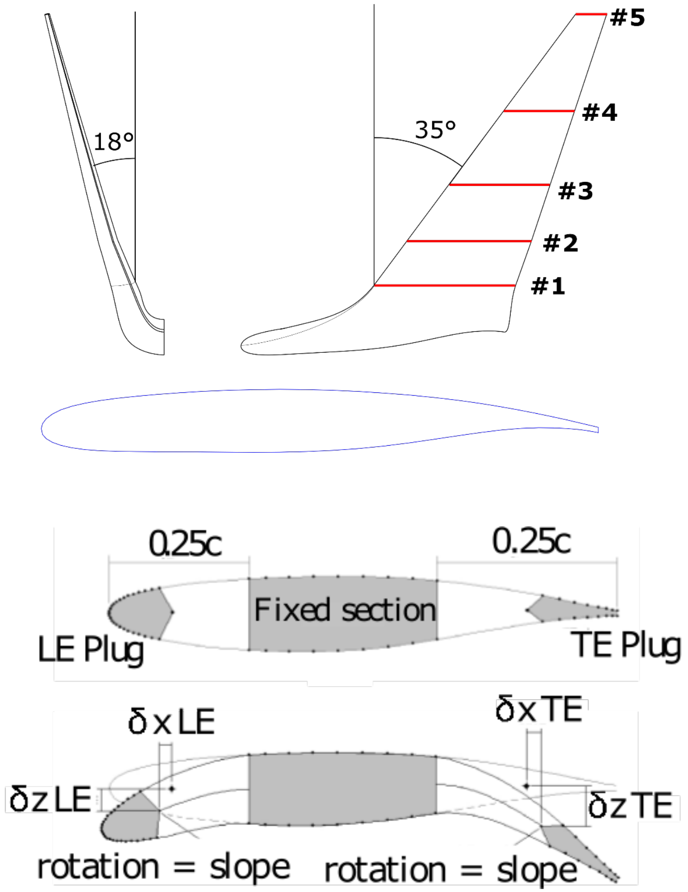

Mission profile

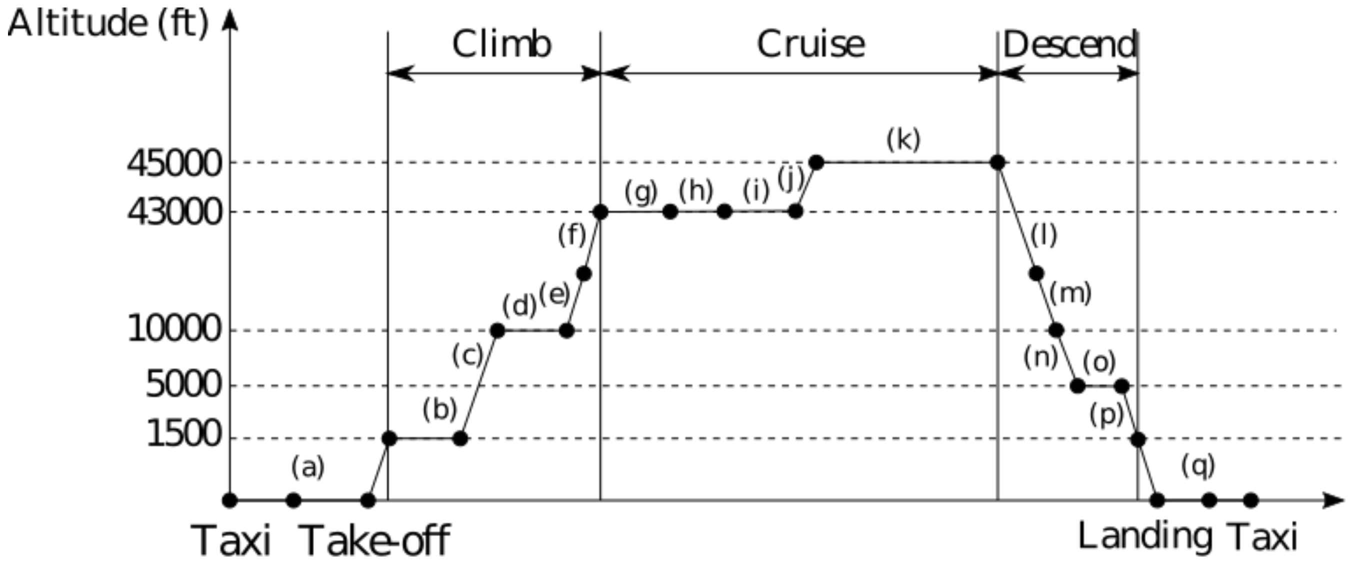

(a) Engine start, warm up, taxi, take-off and climb to 1500 ft. The weight at the end of this phase is considered to be $W_{to} = 0.98TOW$

(b) Acceleration from $Mach = 0.3$ to $IAS = 154\frac{m}{s}$ at $h = 1500$ ft.

(c) Climb at constant $IAS = 154\frac{m}{s}$ from 1500 ft to 10000 ft.

(d) Acceleration from $IAS = 154\frac{m}{s}$ to $IAS = 165\frac{m}{s}$ at $h = 10000$ ft.

(e) Climb at constant $IAS = 165\frac{m}{s}$ from 10000 ft until $Mach = 0.8$.

(f) Climb at constant $Mach = 0.8$ to $h = 43000$ ft.

(g) Cruise at $Mach = 0.8$ and $h = 43000$ ft.

(h) Acceleration from $Mach = 0.8$ to $Mach = 0.8124$ at $h = 43000$ ft.

(i) Cruise at $Mach = 0.8124$ and $h = 43000$ ft.

(j) Climb from $h = 43000$ ft to $h = 45000$ ft at $M = 0.8124$.

(k) Cruise at $Mach = 0.8124$ and $h = 45000$ ft.

(l) Descent from $h = 45000$ ft at constant $M = 0.8$ until $IAS = 165\frac{m}{s}$.

(m) Descent to $h = 10000$ ft at constant $IAS = 165\frac{m}{s}$.

(n) Descent to $h = 5000$ ft at constant $IAS = 154\frac{m}{s}$.

(o) Loiter at $h = 5000$ ft for $t_{loit} = 30$ min

(p) Descent from $h = 5000$ ft to $h = 1500$ ft at constant $IAS = 154\frac{m}{s}$.

(q) Landing from 1500 ft, taxi and engine shut down. It is considered a weight at the end of the taxi as $W_{ld} = 0.992W_i$

Performance model

$$RoC = \frac{\frac{(T-D)V}{W}}{1+\frac{V}{g}\frac{dV}{dh}}$$

$$R = \frac{a_0\sqrt{\frac{\tau}{\tau_0}}}{TSFC} Mach \frac{C_L}{C_D} \ln\frac{W_{initial}}{W_{final}}$$

$$RoD = -\frac{\frac{(T-D)V}{W}}{1+\frac{V}{g}\left(\frac{-dV}{dh}\right)}$$

T_{max} [N]	$T_{max_{cont}}$ [-]	T_{idle} [-]	$TSFC_0$ [$\frac{kg}{Ns}$]
62600	$0.625T_{max_{av}}$	$0.06T_{max_{av}}$	1.859×10^{-5}

- For constant IAS climb

  $$\frac{dV}{dh} = 0.567M^2$$

- For constant Mach climb

  $$\frac{dV}{dh} = -0.133M^2$$

$$T_{max_{av}} = T_{max}\left(\frac{\rho}{\rho_0}\right)^{0.7}$$

$$TSFC = TSFC_0\sqrt{\frac{T}{T_0}}M^{0.48}$$

$$\Delta W = -TSFC \times T \times dt$$

Genetic algorithm optimization

CMWlet

$$\underset{P_{le_i},\,P_{te_j}}{\text{maximize}}\ F\left(P_{le_i}, P_{te_j}\right) = \frac{C_L}{C_D}\left(P_{le_i}, P_{te_j}\right)$$

$$\text{subject to} \quad -2.45 \le P_{le_i} \le 1.3$$
$$-0.1 \le P_{te_j} \le 0.05$$

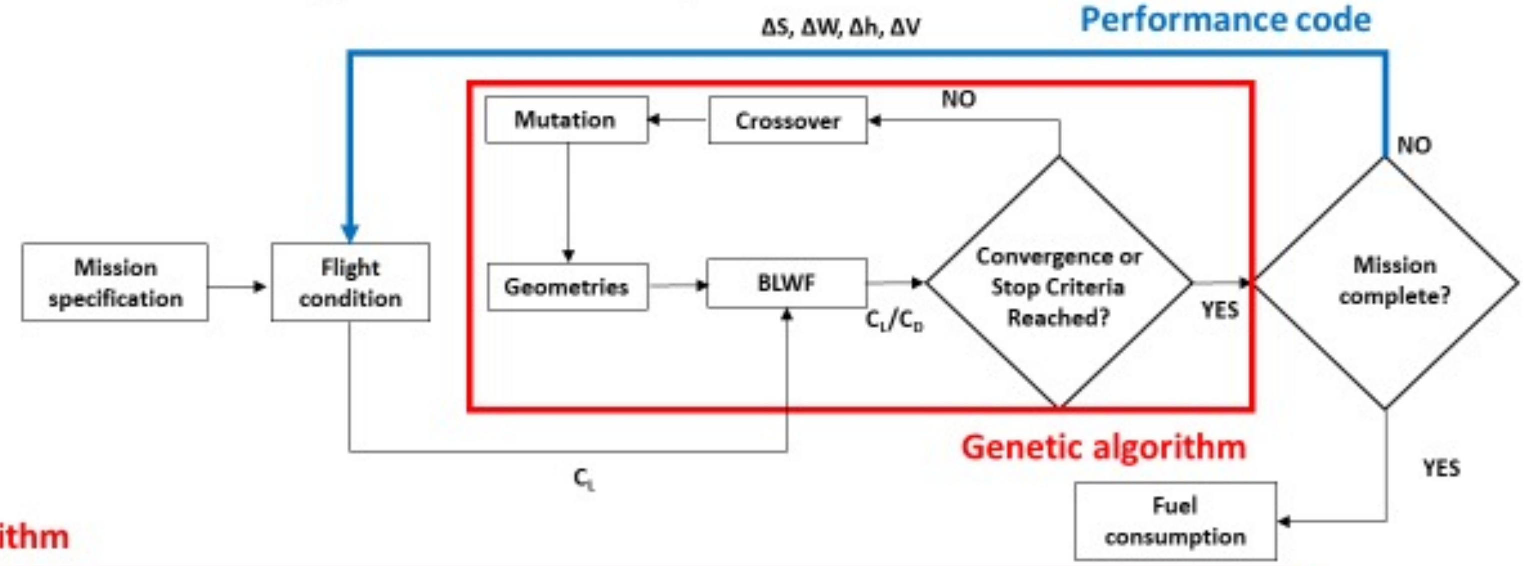

Fixed Wlet

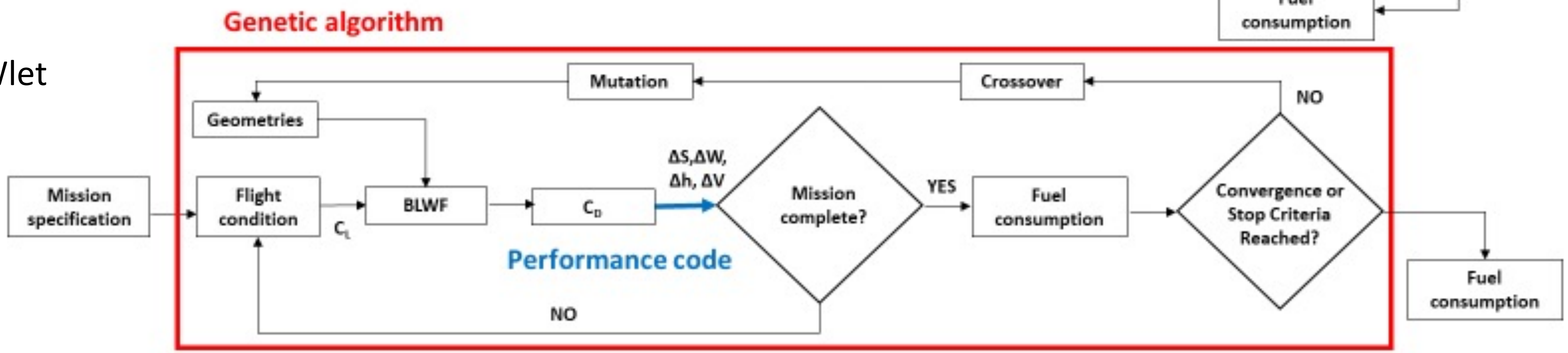

Performance improvement

	FGW	CMW	Δ [%]
Time to climb (@ 430 FL) [min]	43	34	−20.9
Climb fuel consumption [kg]	540	445	−17.6
Cruise time [h]	6.25	6.25	0.0
Cruise fuel consumption [kg]	3590	3390	−5.9
Mission fuel consumption [kg]	4655	4355	−6.0

$h = 1500$ ft
$IAS = 99.34$ m/s
$M = 0.30$

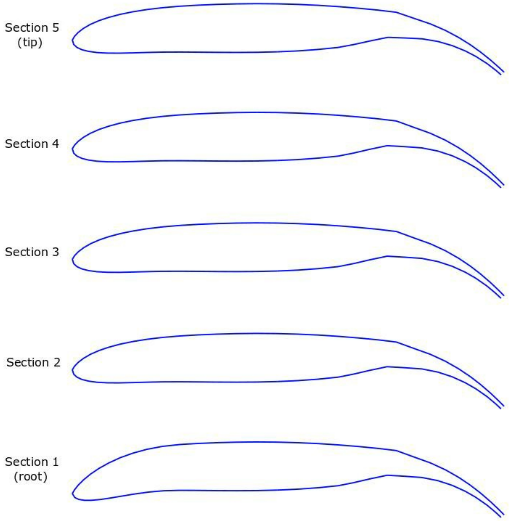

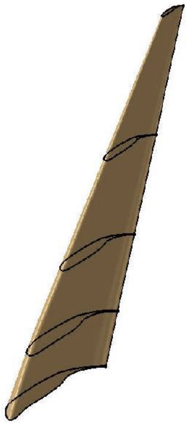

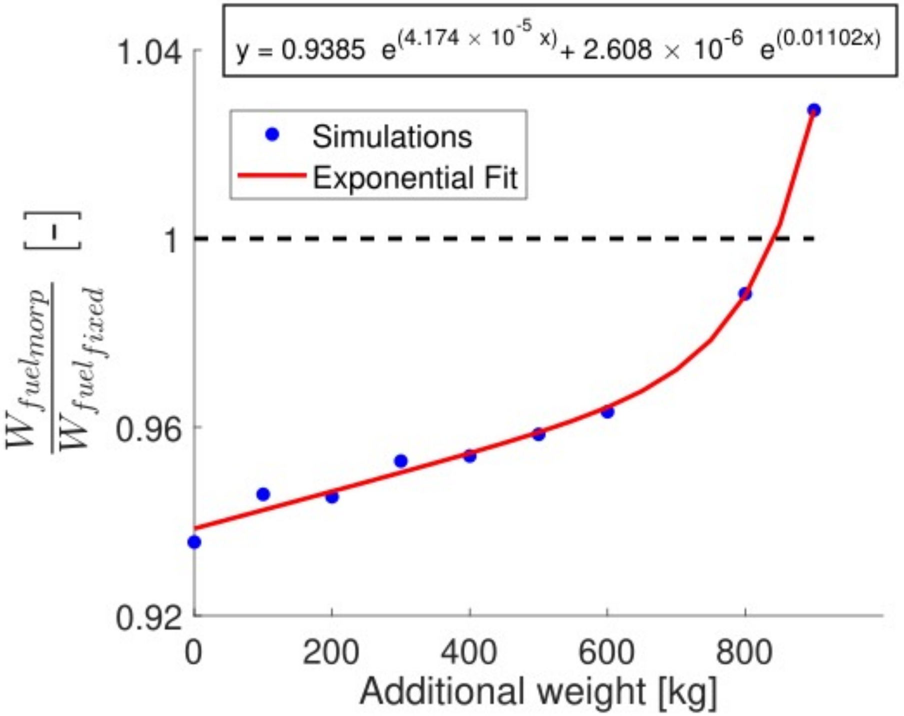

Drag breakdown

Condition	H [ft]	M [-]	Re [x10^6]	C_L
Cruise 1	43000	0.8000	11.1	0.471
Cruise 2	43000	0.8124	11.2	0.408
Climb 3	45000	0.8124	10.2	0.383

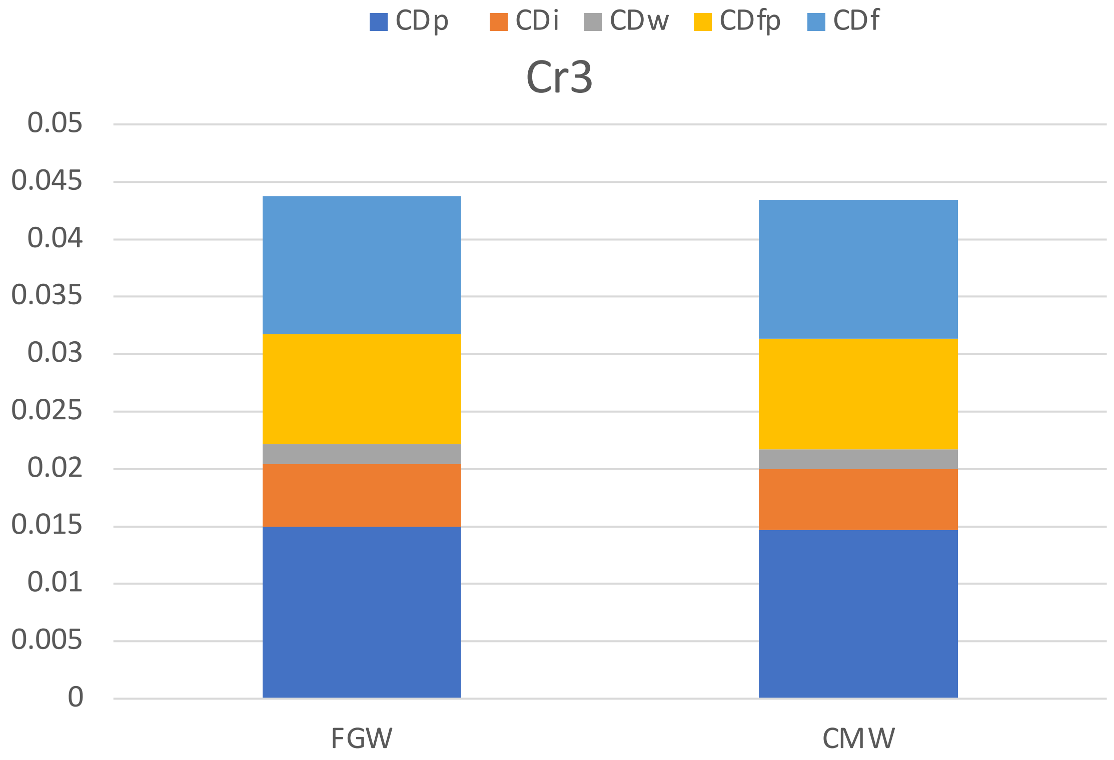

$C_D = 0.04377$ $C_D = 0.04340$

Drag breakdown

Condition	h [ft]	M [-]	Re [x10^6]
Climb 1 (Cb_1)	6100	0.5069	25.4
Climb 2 (Cb_2)	20590	0.7242	23.5

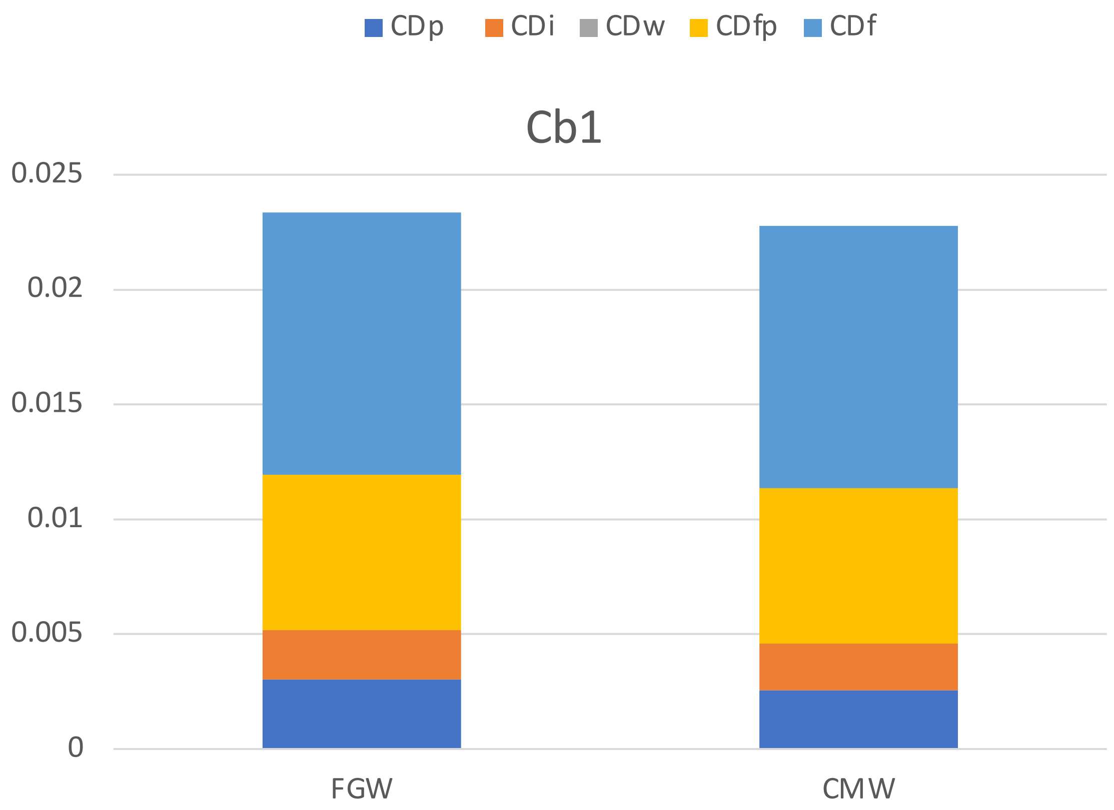

$C_D = 0.02336$ $C_D = 0.02278$

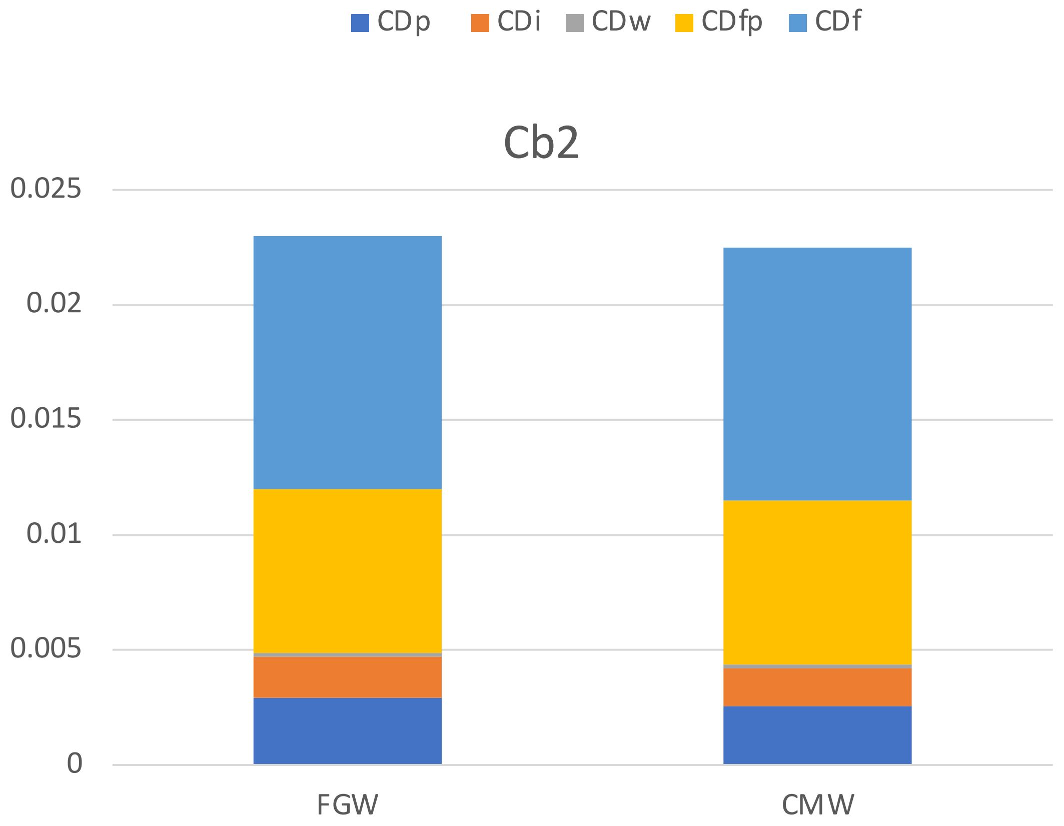

$C_D = 0.02300$ $C_D = 0.02250$

Condition	h [ft]	M [-]	Re [x10^6]
Cruise 1 (Cr_1)	43000	0.8000	11.1
Cruise 2 (Cr_2)	43000	0.8124	11.2
Cruise 3 (Cr_3)	45000	0.8124	10.2

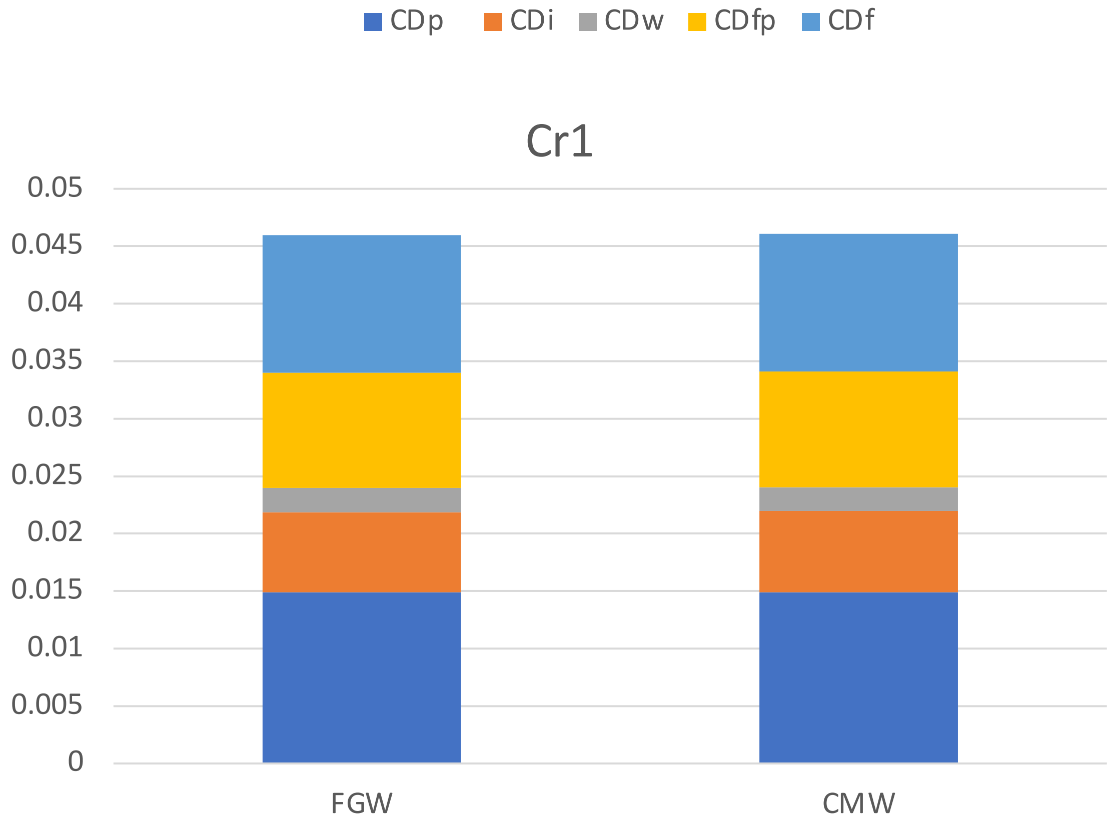

$C_D = 0.04597$ $C_D = 0.04607$

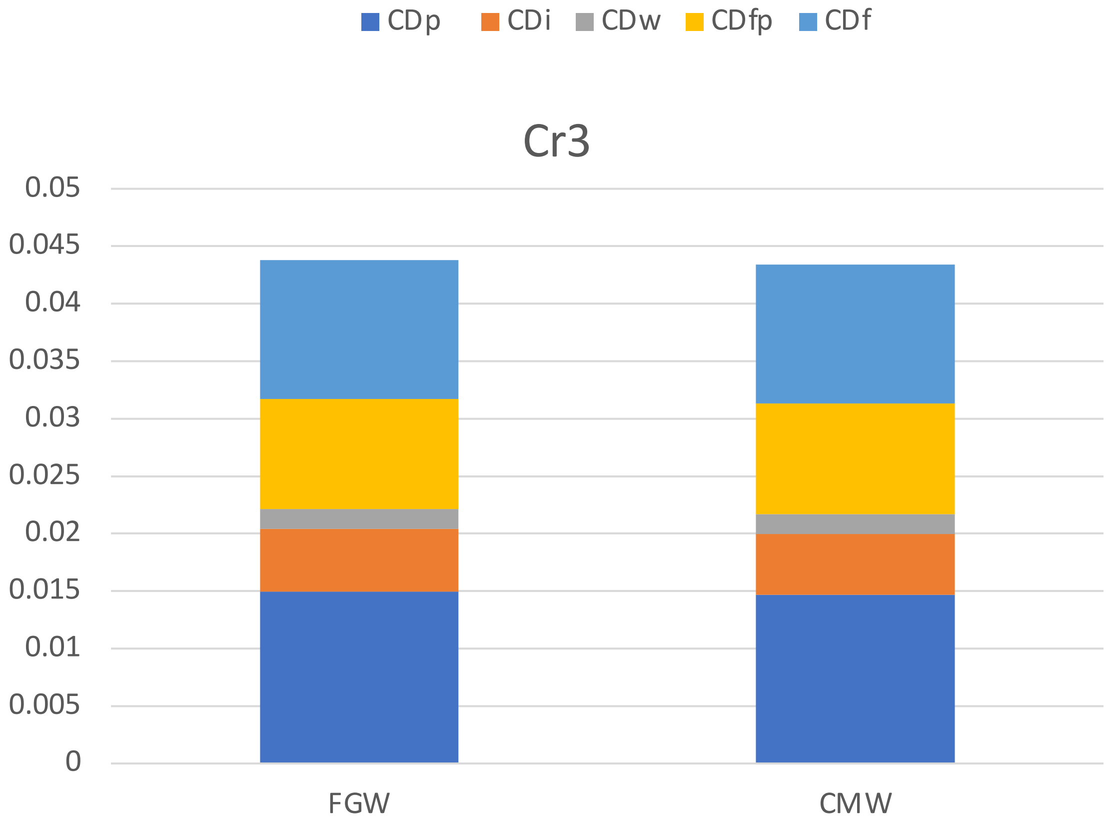

$C_D = 0.04377$ $C_D = 0.04340$

Drag breakdown

	Mach	Reynolds ($x10^6$)	C_L	% ΔC_{Di}	% ΔC_{Dp}	% ΔC_{Dw}	% ΔC_D	% Δ L/D
Climb 1	0.50	25.4	0.251	-5.60	-15.51	0	-2.48	2.54
Climb 2	0.72	23.5	0.217	-7.86	-12.37	0	-2.17	2.22
Cruise 1	0.80	11.1	0.471	0.71	0.20	0.48	0.217	-0.21
Cruise 3	0.8124	10.2	0.383	-2.57	-1.93	-0.57	-0.84	0.85

CFD simulations

- RANS simulations
- Unstructured grids
- Evaluate the accuracy of the full-potential method code
- CFD results explored how the camber morphing winglet affects the aircraft performance and tip vortex structure

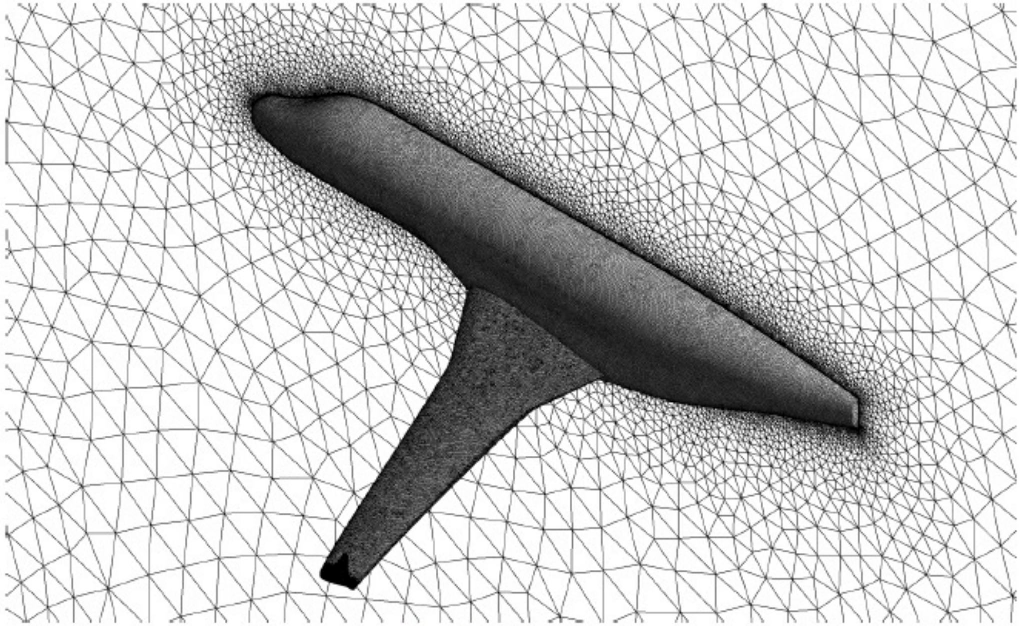

(a) Mesh global view.

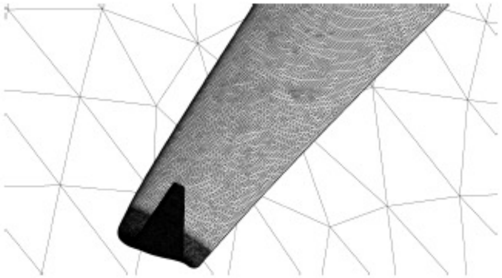

(b) Close-up view for winglet mesh refinement.

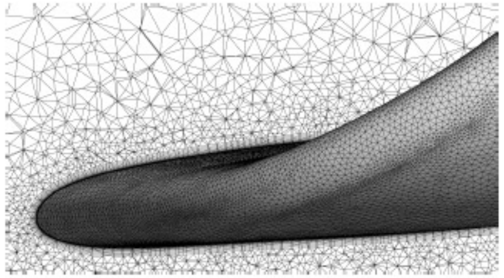

(c) Close-up view of boundary layer prism on winglet.

Vortex structure

- Data for climb condition.
- A similar behavior at cruise condition

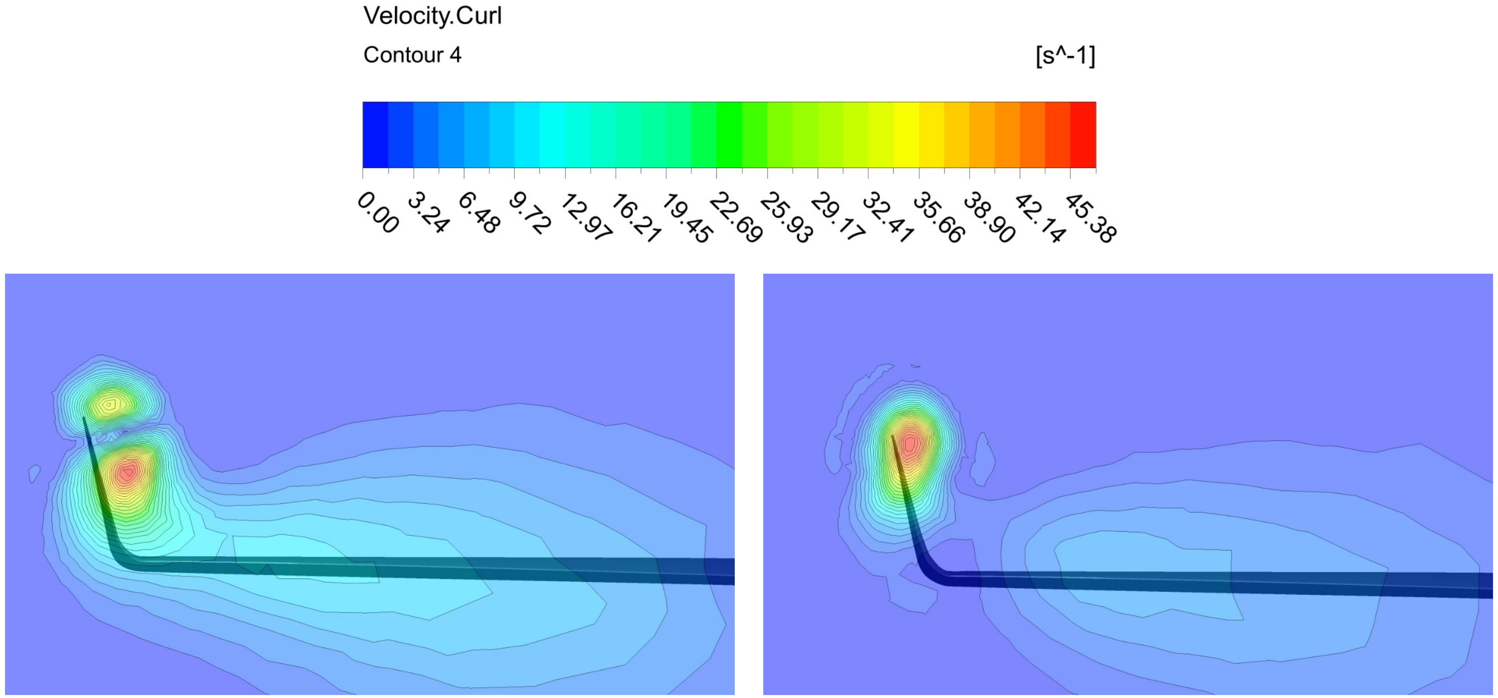

(a) Baseline winglet. (b) Optimized winglet.

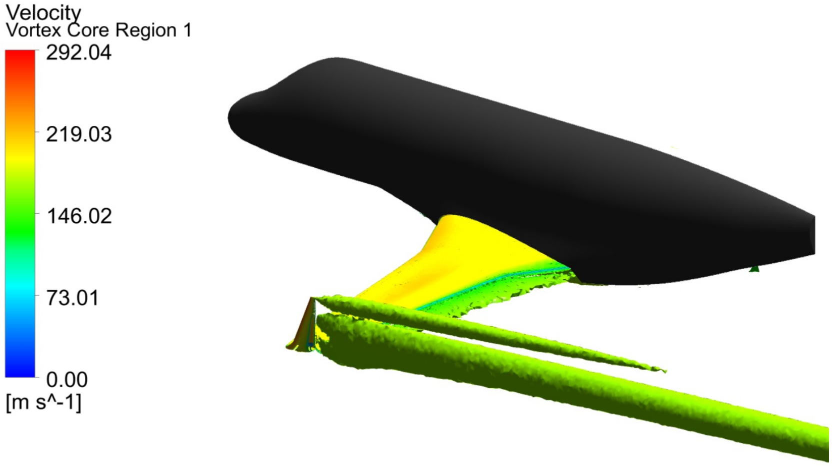

(a) Baseline winglet.

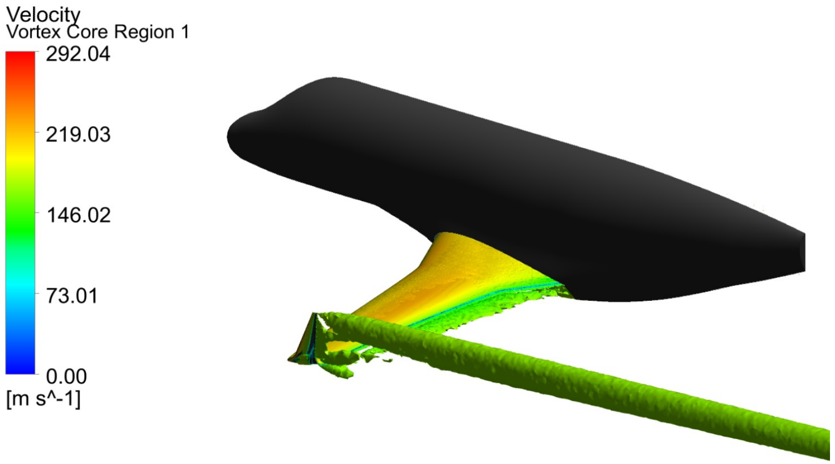

(b) Optimized winglet.

Streamlines

- Climb condition.

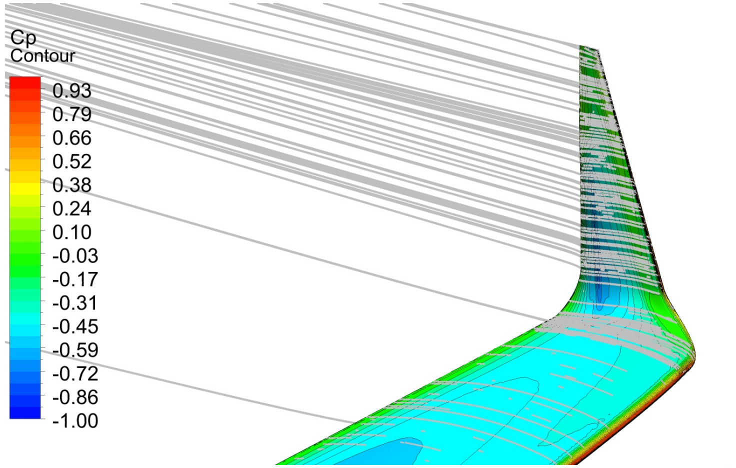

(a) Baseline winglet.

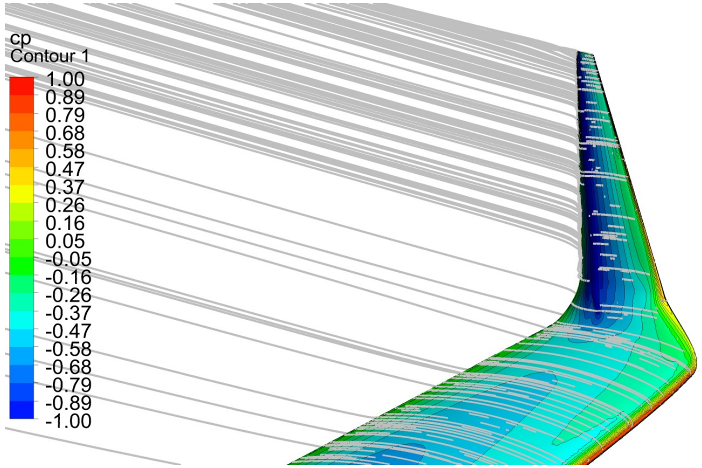

(b) Optimized winglet.

- Cruise condition

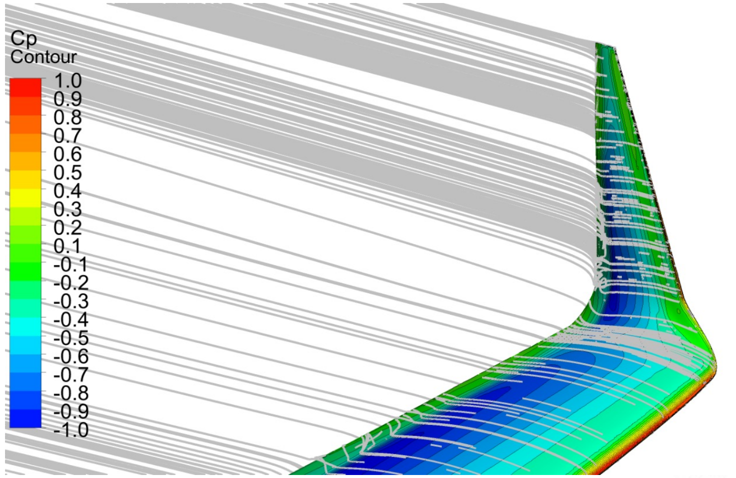

(a) Baseline winglet.

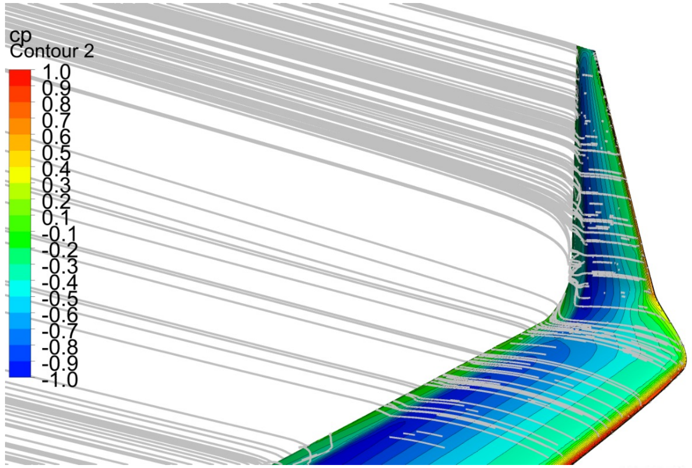

(b) Optimized winglet.

Pressure distribution

- Climb condition.

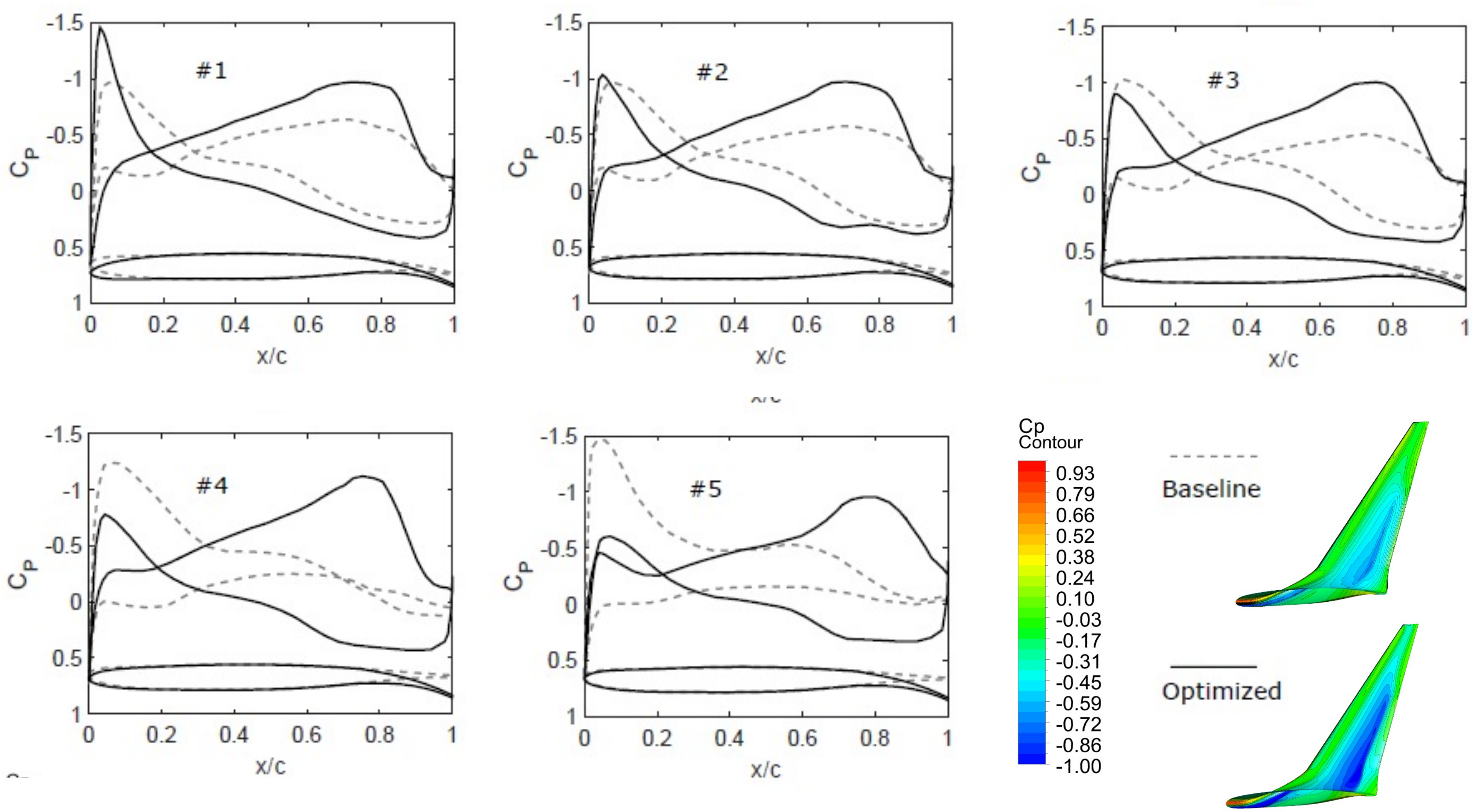

Pressure distribution

- Cruise condition.

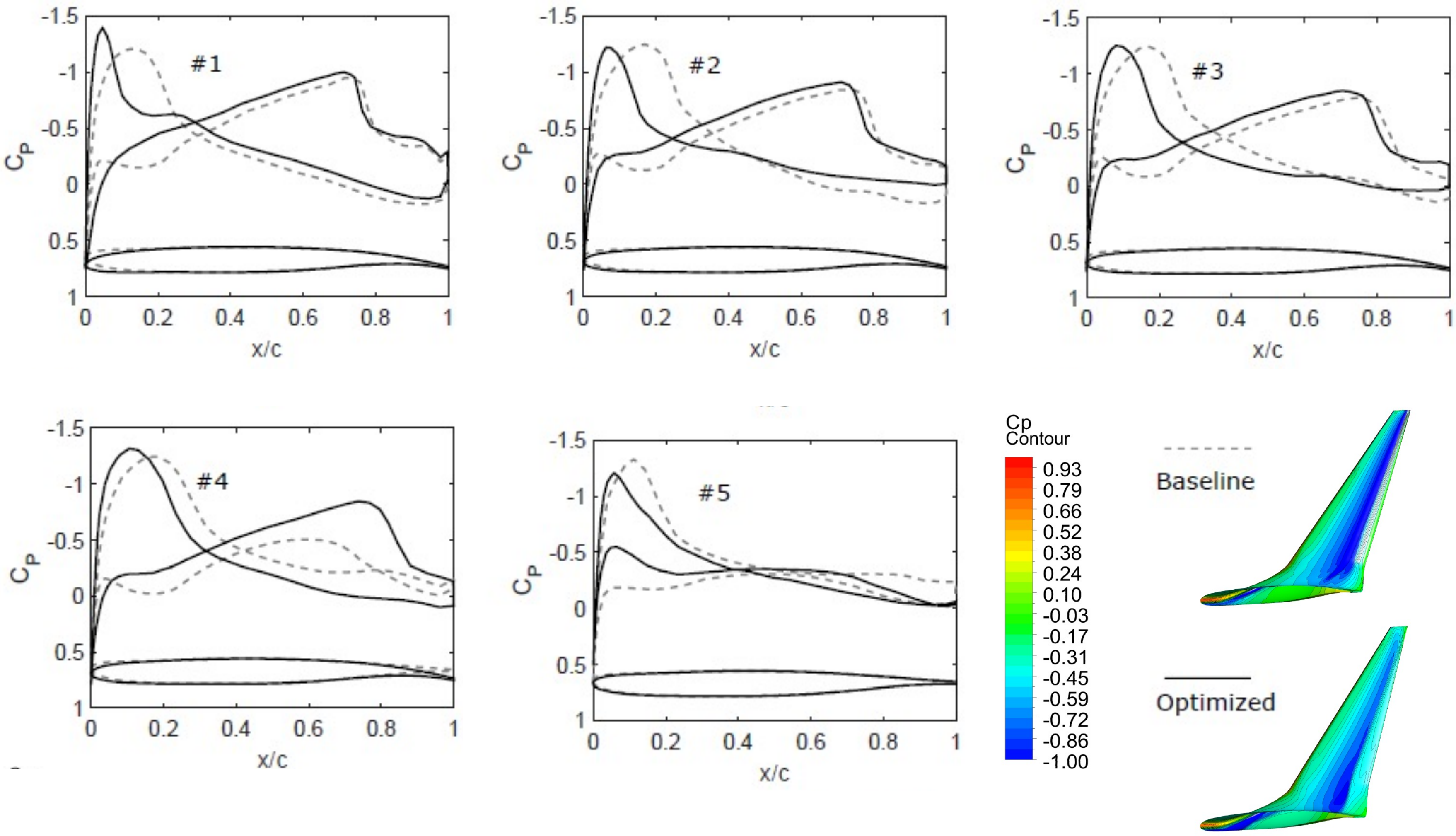

Conclusions

- This work aimed to evaluate the impact of a medium-fidelity method (BLWF code) on the evaluation of a camber morphing winglet (CMW) against high-fidelity results from CFD package.
- The results validate both the BLWF code as a valuable tool for conceptual and preliminary investigation of innovative configurations and the performance improvement due to the CMW.
- The drag breakdown investigation shows that the camber morphing winglet reduces induced and pressure drag as compared to a fixed geometry winglet. The vorticity and streamlines provided a qualitative and quantitative explanation of the induced drag reduction.
- The winglet sections pressure distributions complemented the analysis by showing how the CMW modified the CP distribution to reduce pressure drag. The presence of a flow separation on climb and weak shock waves on cruise were found near the winglet sections trailing edges. However, the separation and shock waves did not affect the aircraft performance.
- Further studies to estimate the camber morphing winglet actuation system's weight and power, evaluations of the structural and aeroelastic impacts, and wind tunnel experiments, are necessary for finishing its proof of concept.